THE JOURNAL OF PHYSICAL CHEMISTRY C
A JOURNAL OF THE AMERICAN CHEMICAL SOCIETY

pubs.acs.org/JPCC

Article

Structure and Reactivity of Pristine and Reduced Spinel $CoFe_2O_4$ (001)/(100) Surfaces

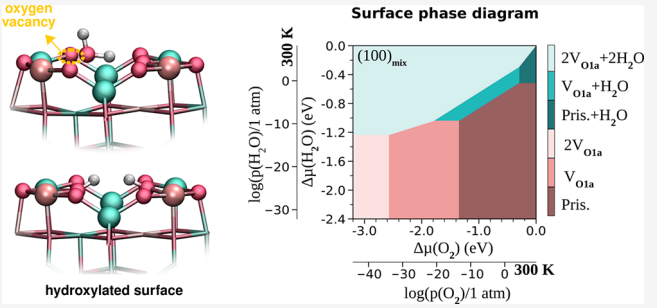
Arjeta Rushiti,* Christof Hättig, Bo Wen, and Annabella Selloni

Cite This: https://doi.org/10.1021/acs.jpcc.1c01881

Read Online

ACCESS | Metrics & More | Article Recommendations | Supporting Information

ABSTRACT: Cobalt ferrite, $CoFe_2O_4$ (CFO), nanocrystals are efficient and competitive anode materials in the field of electrochemical water splitting. Using density functional theory with on-site Hubbard U corrections (DFT+U), we have investigated the structural, electronic, and magnetic properties of CFO (001)/(100) surfaces, as well as their reactivities toward water adsorption. Special attention has been focused on the formation of oxygen vacancies (V_O), due to their key role in the oxidation activity of metal oxides, often based on the Mars–van Krevelen mechanism. Our results show that vacancy formation is easiest at oxygen sites that are not bound to tetrahedrally coordinated Fe. Water adsorbs mainly in molecular form on the Co/Fe metal cations, whereas it dissociates at defects. In comparison to other spinels, CFO is similar to $NiFe_2O_4$, exhibiting relatively low energy cost of V_O formation and a strong affinity of the vacancies toward water. These findings suggest that CFO may be a more promising oxidation catalyst than $NiCo_2O_4$ and Co_3O_4.



INTRODUCTION

Metal oxides with the spinel structure are of great interest in the field of catalysis due to a combination of desirable properties including chemical and thermal stability, suitable band gap, cation miscibility, and multiple oxidation states.[1−3] In particular, the spinel ferrites, with the general formula AFe_2O_4, have emerged as promising sustainable materials for the oxygen evolution (OER) and oxygen reduction (ORR) reactions,[4,5] methane complete oxidation,[6] and the water-gas shift (WGS) reaction,[7,8] in which CO and water vapor react to form CO_2 and H_2.

One such interesting spinel ferrite derivative is cobalt ferrite, $CoFe_2O_4$ (CFO), an insulating material with a high magnetic ordering temperature. Experimentally, CFO is found to be an inverse spinel, even though the degree of inversion is not complete, between 0.76 and 0.93, depending on sample preparation.[9,10] The metal cations are distributed over tetrahedral (T_d) and octahedral (O_h) sites within the fcc oxygen sublattices, such that half of the most abundant cation species (Fe^{3+}) occupy the T_d sites, whereas the occupation of the O_h sites is split in half by the remaining Fe^{3+} ions and the divalent metal cations (here Co^{2+}).

Over the past decade, most research on CFO has been focused on its use as an anode material in the field of electrochemical water splitting. A combined experimental and theoretical study[11] has reported enhanced catalytic activity toward OER of CFO nanoparticles with a small size (3.1 nm) and of CFO nanoparticles with partial substitution of Co with Ni. Another combined study[12] explored the role of vanadium substitution and reported that phase-pure $CoV_{2-x}Fe_xO_4$ (with $0 \le x \le 2$) is a promising bifunctional electrocatalyst with high catalytic activity for both OER and ORR. Recently, the performance of $Co_xNi_{1-x}Fe_2O_4$ (001) (with x = 0.0, 0.5, 1.0) for water oxidation has been investigated theoretically with a focus on the effects of surface termination and cation substitution.[13] The study shows how selective surface modification can affect the catalytic performance of such materials. Furthermore, there is an extensive ongoing comparative research on mixed cobalt-iron oxides of the spinel and perovskite types, aiming at a fundamental understanding of the redox chemistry of these materials in heterogeneous catalysis.[14−17]

To contribute to this growing area of research, in this work, we present a theoretical study of the CFO (001) surfaces with exposed $Co(O_h)$ and $Fe(O_h)$ ions, and the mixed (100) surface which exposes both $Co(O_h)/Fe(O_h)$ ions. Using first-principles density functional theory (DFT) calculations, we investigate the geometric and electronic structure properties as well as the chemical trends arising from defects. In particular, we study the formation and stability of oxygen vacancies, as these have a crucial influence on the redox properties of oxide surfaces based on the Mars–van Krevelen (MvK) mecha-

Received: March 2, 2021
Revised: April 23, 2021

Downloaded via BOCHUM LIBRARIES on May 10, 2021 at 07:36:38 (UTC).
See https://pubs.acs.org/sharingguidelines for options on how to legitimately share published articles.

ACS Publications
© XXXX American Chemical Society

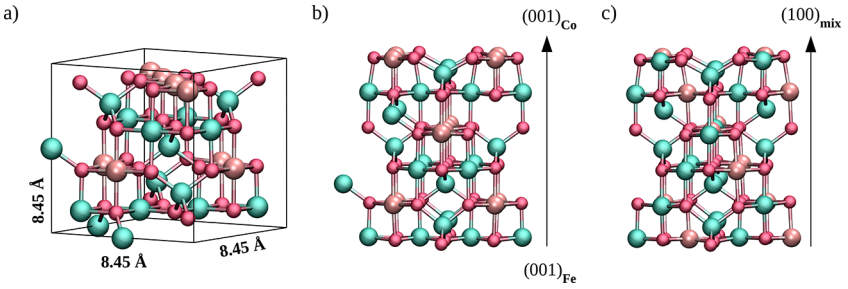


Figure 1. Structures of the (a) bulk conventional cubic cell and the 11-layer (b) (001) and (c) (100) surface cells of cobalt ferrite. The (001) termination is asymmetric and exposes Co ions (nude spheres) and Fe ions (green spheres), on opposite sides. The (100) termination exposes a mixed layer of the metal cations. Oxygen anions are represented by red spheres.

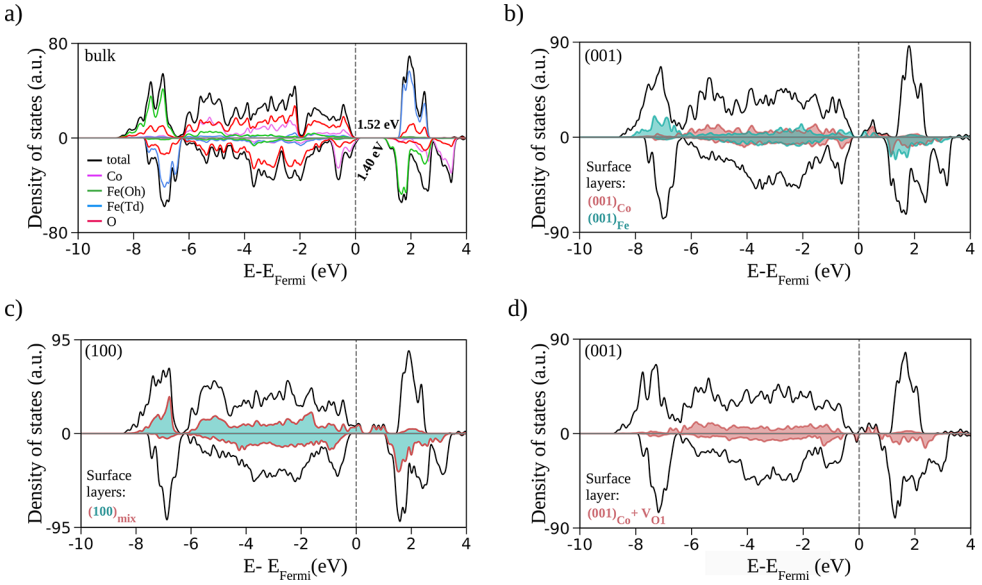


Figure 2. (a) Projected density of states for bulk CFO. Total and surface layer-resolved density of states for the (b) (001) and (c) (100) pristine slabs and the (d) (001) slab with an O1 vacancy on the $(001)_{Co}$ surface.

nism.[18] To characterize the reactivity of the considered pristine and reduced surfaces, we study the adsorption of a single water molecule and identify the vacancies as strongly binding adsorption sites. Finally, we compare CFO to other spinels such as nickel ferrite, $NiFe_2O_4$ (NFO), nickel cobaltite, $NiCo_2O_4$ (NCO), and cobalt oxide, Co_3O_4, with similar catalytic activity and of technological interest.

■ COMPUTATIONAL METHODS

Spin-polarized DFT calculations were carried out with the Quantum Espresso package[19] which uses the plane-wave-pseudopotential scheme. The gradient corrected Perdew–Burke–Ernzerhof (PBE)[20] functional was used in combination with the on-site Coulomb repulsion U term to take into account the exchange and static correlations of the Co and Fe 3d electrons. We used values of 3.0, 3.4, and 3.5 eV for Co, Fe(T_d), and Fe(O_h), respectively, which have been found to provide a good description of the thermodynamic properties in other ferrite and Co-containing spinels.[21,22] The core electrons, O: 1s and Co/Fe: 1s, 2s, 2p, were accounted for using ultrasoft pseudopotentials.[23] Relaxation of the atomic positions was carried out until the residual forces were smaller than 1×10^{-3} ha/bohr. For wave functions and augmented densities, kinetic energy cutoffs of 35 and 350 Ry, respectively, were employed.

Bulk calculations were performed using a conventional cubic cell. This is a $\sqrt{2} \times \sqrt{2} \times 1$ primitive cell containing 8 formula units and 56 atoms, in total. The Brillouin zone was sampled using a $2 \times 2 \times 2$ Monkhorst–Pack k-point grid.

Surface properties were studied for the β-type inverse spinel only, which has already been identified to be more favorable than the α-type.[13,24] Surfaces were simulated using non-symmetric slabs of 11 layers. To avoid interaction, the adjacent slabs were separated by a vacuum region of 20 Å. The Brillouin zone was sampled using a $2 \times 2 \times 1$ k-point grid.

Dipole corrections for the pristine and defected non-symmetric slabs, with and without adsorbate, were found to have an effect of less than 0.01 eV in the total energies and, thus, were neglected in the standard setup.

Surface defects were investigated by removing oxygen atoms on one surface. The formation energy for the oxygen vacancies was calculated using the following relation

$$E_{form} = \left(E_{def} + \frac{n}{2}\mu(O_2) - E_{pris}\right)/n \quad (1)$$

where E_{def} and E_{pris} denote the defected and pristine surfaces, respectively, n is the number of oxygen vacancies, and $\mu(O_2)$ is the chemical potential of O_2.

Similarly, adsorption calculations were performed by introducing a single water molecule on one side of the slab.

https://doi.org/10.1021/acs.jpcc.1c01881
J. Phys. Chem. C XXXX, XXX, XXX−XXX

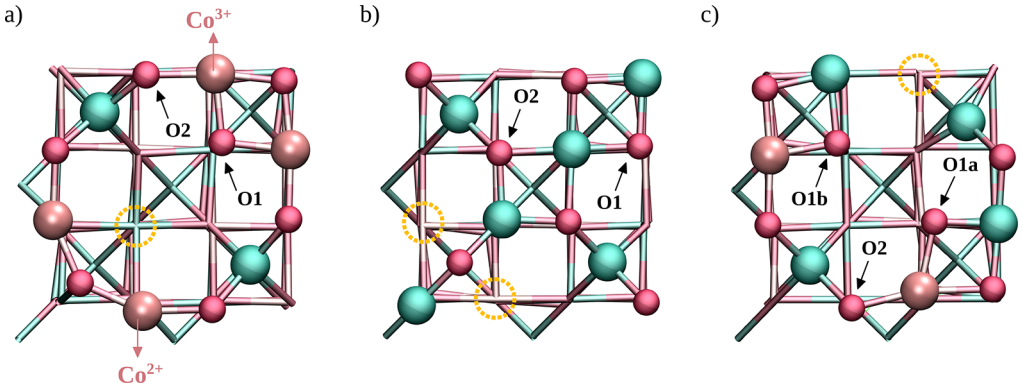


Figure 3. Top view of the defected surfaces. (a) O1 vacancy on $(001)_{Co}$ reduces $Co(O_h)$. (b) O1 split-vacancy on $(001)_{Fe}$. (c) O2 vacancy on $(001)_{mix}$ results in under-coordinated $Fe(T_d)$. Oxygen vacancies are marked with yellow circles. The different types of oxygens are defined in the text.

The adsorption Gibbs free energy, which we will refer to as simply "adsorption energy" from now on, was calculated as

$$E_{ads} = E_{surf+H_2O} - E_{surf} - \mu(H_2O) \quad (2)$$

with E_{surf+H_2O} and E_{surf} denoting the total energies of the surfaces with and without water, respectively, and $\mu(H_2O)$ accounting for the chemical potential of H_2O in gas phase. The chemical potentials of O_2 and H_2O were obtained from values of gas phase enthalpies (H) and entropies (S), tabulated in the JANAF thermochemical tables,[25] using the relation for the Gibbs free energy ($G = H - TS$) as explained in ref 26.

RESULTS AND DISCUSSION

Bulk Properties. CFO is perfectly cubic and belongs to the $Fd\bar{3}m$ space group (No. 227). We obtain a lattice constant of 8.45 Å for the conventional cubic cell (Figure 1a), which is about 0.72% larger than the experimental value of 8.39 Å.[27]

The computed density of states (DOS), shown in Figure 2a, reveals a band gap of 1.52 and 1.40 eV for the majority spin-up and minority spin-down, respectively, correctly describing CFO as an intermediate-gap insulator, and in good agreement with the reported experimental values ranging between 1.30 and 1.58 eV.[28,29]

Furthermore, consistent with previous studies,[30] we find that CFO exhibits a weak crystal field splitting. Both Co and Fe are found in their high-spin configurations, resulting in a Néel-type ferrimagnetic arrangement. The five unpaired spin-up electrons on $Fe(T_d)$ cancel the magnetic moments of the five unpaired spin-down electrons on $Fe(O_h)$. This results in a magnetic moment of 3.09 μ_B per formula unit, which is attributed to the three unpaired spins-up on the Co^{2+} ion. The different spin states of the metal sites are presented in Table S1 of the Supporting Information.

Surface Properties. *Pristine Surfaces.* The structures of the pristine CFO (001) and (100) slabs considered in this study are presented in Figure 1b,c, respectively.

Although the two slabs have the same overall stoichiometry $Co_{12}Fe_{22}O_{48}$, the (001) and (100) terminations are inequivalent. The (001) slab comprises alternating layers of Co^{2+} and Fe^{3+} ions on the O_h sites: it exposes four $Co(O_h)$ cations and eight oxygens per surface unit cell on one side and four $Fe(O_h)$ cations and eight oxygens on the other side. We refer to these surfaces as $(001)_{Co}$ and $(001)_{Fe}$, respectively. The (100) slab exposes mixed layers of $-Co(O_h)-O-$ and $-Fe(O_h)-O-$ on both sides. We, thus, refer to this surface as $(100)_{mix}$.

Creation of the aforementioned surfaces from the three-dimensional bulk lattice leads to a decreased coordination for the surface sites. To lower the surface energy, the ions undergo small displacements away from their ideal bulk-like positions. Average displacements of the outermost first and second layer atoms from their corresponding positions in the bulk are reported in Table S2 of the Supporting Information. The metal cations tend to have larger out-of-plane displacements, whereas the oxygens show larger in-plane displacements. In the (001) slab, the metal cations of the first layer ($Co(O_h)$ and $Fe(O_h)$) move inward, whereas the outermost oxygen anions are vertically displaced in the opposite direction, moving outward. This is common for surfaces that contain at least two different types of atoms and can be attributed to the electrostatic forces. Such rumpling is also associated with changes in interatomic distances. The Co−O equatorial bonds are contracted (1.94 Å) in comparison to the bulk (2.08 Å), whereas the axial Co−O bonds remain at 2.11 Å, leading to structural distortions for the 5-fold coordinated $Co(O_h)$, similar to Jahn−Teller distortions for nonlinear molecular systems.

To obtain insight into the surface induced changes of the electronic structure, we compare the DOS of the (001)/(100) slabs, in Figure 2b,c, to the DOS of the bulk CFO, in Figure 2a. The DOS for the (001)/(100) terminated slabs shows new empty states in the band gap for the majority spin-up channel, which may in part be related to the nonperfect overall stoichiometry of the slab. The layer-resolved DOS clearly shows that these are surface states that arise from the atomic layers closest to the surface.

The stabilization of the CFO (001)/(100) polar surfaces involves a charge redistribution in the surface layers. We determined the oxidation states for the different metal ions based on the computed spin-up and spin-down d-occupation numbers and the corresponding local magnetic moments.[31−33] The 5-fold coordinated $Co(O_h)$ ions at both the $(001)_{Co}$ and $(100)_{mix}$ surfaces have lower atomic magnetic moments (1.9 μ_B) than in the middle layers (2.5 μ_B), suggesting an oxidation state of +3 with an intermediate spin configuration (Table S1 of Supporting Information). The integrated local density of states for the $(100)_{mix}$ surface in the gap region (Figure S1 of Supporting Information) reveals that the empty surface states are distributed mostly around the under-coordinated lattice oxygens. The 5-fold coordinated $Fe(O_h)$ ions and $Fe(T_d)$ ions in the second layer keep their bulk oxidation states. The same holds for the ions in the middle layers. For the $(100)_{mix}$

https://doi.org/10.1021/acs.jpcc.1c01881
J. Phys. Chem. C XXXX, XXX, XXX−XXX

termination, the atomic magnetic moments of surface Fe(O_h), 3.6 μ_B, fall between the values for the magnetic moments of surface Fe(O_h) on $(001)_{Fe}$, 3.4−3.8 μ_B.

Defected Surfaces. We computed the formation energies of oxygen vacancies (V_Os) on the CFO (001)/(100) surfaces considering 1 and 2 V_Os per surface unit cell, which correspond to coverages of 1/8 and 1/4 monolayer (ML), respectively. As for other inverse spinels, there are two types of oxygen atoms, O1 and O2, on the CFO (001)/(100) surfaces (see Figure 3). Both types are bonded to two 5-fold coordinated metal cations in the outermost layer. The O1 atom is additionally bonded to an octahedrally coordinated metal cation in the third layer. Depending on whether the third layer metal cation is Co(O_h) or Fe(O_h), for the $(100)_{mix}$ surface, we further differentiate between O1a and O1b, respectively. The O2 atom is additionally bonded to the Fe(T_d) cation in the second layer.

The energy costs for the formation of the oxygen vacancies in standard and ambient conditions are summarized in Table 1.

Table 1. Average Oxygen Vacancy Formation Energies for the Different Oxygen and (001)/(100) Surface Types in CFO[a]

	formation energy (eV)	
oxygen type	T = 0 K, p = 1.00 atm	T = 300 K, p = 0.20 atm
	$(001)_{Co}$	
O1	0.53	0.24
O2	2.09	1.79
2 × O1	0.93	0.64
	$(001)_{Fe}$	
O1	0.52	0.22
O2	2.33	2.04
2 × O1	1.01	0.72
	$(100)_{mix}$	
O1a	0.67	0.37
O1b	0.72	0.42
O2	2.24	1.95
2 × O1a	0.98	0.68
2 × O1b	1.00	0.71
O1a - O1b	0.96	0.66

[a]Energies correspond to coverages of 1/8 and 1/4 monolayer (one and two vacancies per surface cell).

Focusing on the values at T = 0 K and p = 1 atm, it becomes clear that removing O2 from any of the considered surfaces of CFO is energetically much more demanding (2.22 eV on average) than removing O1. Identical behavior has been observed for the corresponding surface terminations in NCO,[34] where the formation energy of an O2 vacancy (1.78 eV on average) is larger than the reported values for V_{O1}. The high energy costs of O2 vacancies can be understood by considering that they reduce the coordination number of Fe(T_d) from 4 to 3, which is quite unfavorable (Figure 3c). Among the different CFO surfaces studied here, the generation of a V_{O1} is easier on the $(001)_{Co}$ and $(001)_{Fe}$ terminations, with nearly identical formation energies of 0.53 and 0.52 eV, respectively. In comparison to NCO, these values fall between the formation energies of V_{O1} on $(001)_{Co}$ (0.40 eV) and $(001)_{Ni}$ (1.38 eV). For the $(100)_{mix}$ surface, instead, it is relatively easier to remove O1a (0.67 eV) and O1b (0.72 eV) from CFO than O1a (1.18 eV) and O1b (0.82 eV) from NCO. This easier formation of oxygen vacancies suggests that CFO may be a better oxidation catalyst than NCO for reactions based on the Mars−van Krevelen mechanism.

Similar to what was found for NFO,[35] another spinel ferrite, the V_{O1} formation energies increase significantly when increasing the concentration of the defects. As can be seen from Table 1, generating a surface with a second O1 vacancy almost doubles the average formation energy per defect. For the $(100)_{mix}$ termination, removing only one O1a requires an energy cost of 0.67 eV, whereas removing two O1a atoms costs 0.98 eV per atom. Reported values for the (100) surface of NFO are 0.34 eV for 1 × V_O/unit cell, and 0.71 eV/vacancy for 2 × V_Os/unit cell. A different behavior was found, instead, for the $(100)_{mix}$ termination of NCO, where the first and second V_O formation energies are similar.

Each removed oxygen atom leaves behind two excess electrons at the surface. As a result, the Fermi level moves up in the band gap and new states appear in the electronic structure. On the $(001)_{Co}$ surface, the excess electrons are distributed between the nearest 5-fold coordinated Co(O_h) ions, reducing their formal ionic charge from +3 to +2 and increasing their magnetization from 1.9 to 2.5 μ_B, whereas the magnetic moments of the other Co(O_h) surface ions decrease slightly to 1.8 μ_B. This is accompanied by a geometric relaxation around the oxygen vacancy, such that the closest O1 atom is displaced more toward the middle of the metal cations. The corresponding optimized structure is presented in Figure 3a. The magnitude of the local relaxation is strongest on the $(001)_{Fe}$ surface, where a "split-vacancy"[36] is observed; that is, the remaining O1 is equally shared and displaced exactly in the middle between the Fe ions, occupying the interstitial space between two vacancies (Figure 3b), as previously found for NCO.[34]

Turning next to the $(100)_{mix}$ termination, which exposes both Co and Fe ions, we again observe that one nearby Co ion traps one of the two electrons from the defect and changes its oxidation state from +3 to +2 (Table S1 of the Supporting Information), whereas the second electron remains delocalized in the surface by the electrostatic interaction of the surrounding ions. From the structural point of view, the local relaxation of the defected $(100)_{mix}$ surface bears a resemblance to that of $(001)_{Co}$. In all the CFO terminations considered, the magnetic moments of the Fe(O_h) ions closest to the vacancy are 3.7 μ_B and the cations underneath the missing oxygen relax away from the created defect.

In summary, the new electronic states arising on the defected surfaces can be attributed to both delocalized surface states and reduced metal oxidation states. For illustration, the density of states for the defected $(001)_{Co}$ surface with one O1 vacancy is shown in Figure 2d.

Water Adsorption. We characterized the reactivity of the (001)/(100) CFO surfaces by studying the adsorption of one water molecule per surface unit cell, which corresponds to a coverage of 1/4 ML relative to the number of exposed metal sites. We identified the Co and Fe metal ions as active sites on the pristine surfaces. For the defected surfaces, we focused on the adsorption of water at the most stable oxygen vacancy site (i.e., the O1 vacancy).

Adsorption on a Metal Site. At T = 0 K, water adsorbs in a molecular form at both the Co and Fe sites of the (001) slab (Figure 4a,b). The adsorption energies, compared in Table 2, indicate a rather strong interaction, in-between physi- and chemisorption. Whereas the electronic structure of Fe and its magnetization are barely influenced by the adsorption, Co

https://doi.org/10.1021/acs.jpcc.1c01881
J. Phys. Chem. C XXXX, XXX, XXX−XXX

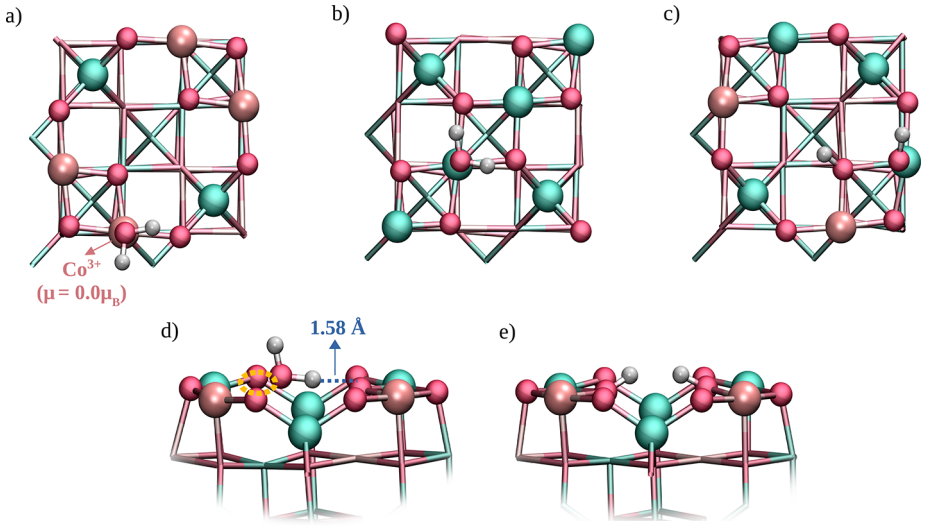


Figure 4. Top view of the molecular adsorption of water on (a) $Co(O_h)$ of $(001)_{Co}$ and (b) $Fe(O_h)$ of $(001)_{Fe}$ pristine surfaces and (c) the dissociative adsorption on $Fe(O_h)$ of $(100)_{mix}$. Side view of the (d) molecular and (e) dissociative adsorption of water at the O1b vacancy of the $(100)_{mix}$ surface. For clarity, only the first and second layer atoms are represented by spheres. The oxygen vacancy is marked by a yellow circle.

Table 2. Water Adsorption Energies on the Metal Sites of the Pristine Surfaces and at the O1 Vacancy Sites of the Reduced Slabs[a,b]

	adsorption Gibbs free energy (eV)	
adsorption site	T = 0 K, p = 1.00 atm	T = 300 K, p = 0.02 atm
	$(001)_{Co}$	
Co (M) - LS[c]	−0.60	−0.02
Co (M) - IS[d]	−0.38	0.20
V_{O1} (M)	−0.63	−0.05
V_{O1} (D)	−0.91	−0.32
	$(001)_{Fe}$	
Fe (M)	−0.70	−0.11
V_{O1} (M)	−0.72	−0.13
V_{O1} (D)	−1.37	−0.78
	$(100)_{mix}$	
Co (M)	−0.47	0.12
Co (D)	−0.40	0.19
Fe (M)	−0.48	0.11
Fe (D)	−0.51	0.07
V_{O1a} (M)	−0.72	−0.14
V_{O1a} (D)	−1.03	−0.44
V_{O1b} (M)	−0.69	−0.11
V_{O1b} (D)	−1.00	−0.41

[a]Energies correspond to a coverage of 1/4 monolayer (single water molecule per surface cell). [b]Molecular and dissociative adsorptions are denoted by (M) and (D), respectively. [c]Low-spin configuration for $Co(O_h)$. [d]Intermediate spin configuration for $Co(O_h)$.

prefers the low-spin state underneath the adsorbate and its magnetization is reduced to zero. Adsorption of a water molecule on a Co with an intermediate spin state (0.38 eV), as found at the clean surface, is indeed 0.22 eV less favorable than on a Co with no magnetization (0.60 eV). The Co−O distance is also larger for the former, with a value of 2.24 Å. Interestingly, a similar behavior was found for the normal spinel Co_3O_4: in a study of selective 2-propanol oxidation over Co_3O_4 nanoparticles, Anke et al.[37] reported that Co has a +3 ionic charge with intermediate spin at the bare surface, but becomes unpolarized underneath both adsorbates, 2-propanol and oxygen. Moreover, this observation corroborates earlier findings,[13] that the magnetization of Co, at the $(001)_{Co}$ surface of CFO, is quenched when certain species are chemisorbed. For comparison, we also considered dissociated water on the defect-free $(001)_{Co}$ surface. Dissociation is found to be 0.15 eV less stable than the molecular adsorption and results in a change of Co's magnetic moment to 0.4 μ_B.

On the $(100)_{mix}$ surface, the molecular and dissociated forms are predicted to coexist in almost equal amounts for the Co and Fe active sites. The dissociation of water on Fe, presented in Figure 4c, is 0.03 eV more favorable than the corresponding molecular adsorption (0.48 eV). The case is opposite for Co, where the molecular adsorption is 0.07 eV more negative than the dissociative adsorption. The electronic structure of the metal centers for water adsorption on $(100)_{mix}$ reflects the same findings as for the (001) slab. The spin occupations of the d-orbitals used to determine the oxidation states for the adsorption sites are given in Table S1 of the Supporting Information.

Adsorption at a Vacancy. As can be seen from Table 2, the molecular adsorption of water, at T = 0 K, is more favorable at the O1 vacancies than on the metal sites. This is especially true for the $(100)_{mix}$ surface, where the adsorption energy is ∼0.20 eV more negative. The optimized structures show a hydrogen bond between the molecularly adsorbed water and the neighboring lattice oxygen of O1 type (Figure 4d), with H−$O_{surface}$ bond lengths between 1.49 and 1.70 Å.

This surface oxygen anion acts as a Brønsted base and can capture the H^+ from water while the deprotonated molecule binds to the surface metal cations. In fact, water always prefers to dissociate at the vacancy (Figure 4e), forming two OH groups consistent with the equation:

$$H_2O + V_O + O_{surface} \rightarrow 2OH_{surface} \quad (3)$$

Somewhat unexpectedly, we find that water adsorption is most favorable at the split-vacancy on the $(001)_{Fe}$ surface, where it tends to heal the V_O reconstruction with an energy gain of 1.37 eV at T = 0 K (0.78 eV at ambient conditions). This result deviates from what was observed for NCO,[34] where the adsorption is less favorable at a split-vacancy site. The higher vacancy reactivity on the $(001)_{Fe}$ surface can be attributed to

https://doi.org/10.1021/acs.jpcc.1c01881
J. Phys. Chem. C XXXX, XXX, XXX−XXX

the more basic character of the under-coordinated oxygen. Consistent with this explanation, the $O1_{surface}$ on $(001)_{Fe}$ shows the strongest affinity to H from water, having the shortest hydrogen bond length of only 1.49 Å, in comparison to those on $(001)_{Co}$ and $(100)_{mix}$.

Surface Phase Diagrams. While the oxygen vacancy is the predominant defect under ultra-high vacuum conditions, it is not so common under ambient conditions, where water readily reacts and dissociates, leading to hydroxylated surfaces. To characterize the structure of the CFO (001)/(100) surfaces, we computed the formation energy of the surfaces in contact with two gases, water and O_2, using the procedure described in ref 35. We combined the energetics of V_{O1} formation (from Table 1) and water adsorption (from Table 2) and additionally considered the dissociation of two water molecules at 2 × V_{O1}s/surface cell (Figure S5 of the Supporting Information).

As shown by the phase stability diagrams in Figure 5, the CFO surfaces considered in this study are hydroxylated under ambient conditions, which correspond to p_{O_2} = 0.2 atm and p_{H_2O} = 0.02 atm saturated vapor at 300 K. More specifically, under ambient conditions, the most stable structure for the $(001)_{Fe}$ and $(100)_{mix}$ surfaces consists of one hydroxyl pair per surface cell (V_{O1}+H_2O). In a wider range of conditions, V_{O1}+H_2O remains more favorable for $(001)_{Fe}$, whereas the $2V_{O1}$+$2H_2O$ structure is more prominent for $(100)_{mix}$. On the contrary, for the $(100)_{Co}$ surface, the structure with two pairs of hydroxyls ($2V_{O1}$+$2H_2O$) always dominates over the dissociation of one water molecule at 1 × V_{O1}.

Hydroxyl formation in CFO is comparable to that in NFO,[35] but opposite to that in NCO,[34] which is predicted to become pristine under ambient conditions. The similarity between CFO and NFO surfaces can be attributed to the lower energy cost of the V_O formation in comparison to NCO.[34]

CONCLUSIONS

Interest in CFO has recently shifted from the study of bulk electronic and magnetic properties toward the understanding of surface structure and reactivity, which are crucial for designing efficient catalysts of technological relevance. This has motivated us to investigate the (001)/(100) terminations of CFO with and without oxygen vacancies, using first-principles calculations based on DFT(PBE)+*U*. Our results show that the formation of oxygen vacancies has a similar energy cost in the different Co/Fe surfaces. In general, oxygens bonded to $Fe(T_d)$ sites are harder to remove, and the energy cost of vacancy formation increases rapidly with their concentration. This behavior is comparable to that previously found for NFO, although V_O formation is still easier on the latter.

On the basis of computed water adsorption energies, we identify the $(001)_{Fe}$ surface as the most reactive CFO termination. Water adsorbs mainly in molecular form on Co and Fe metal sites of defect-free surfaces, whereas it always dissociates at oxygen vacancies, healing the reconstructions introduced by the defects and resulting in hydroxylated surfaces. In the bulk and near a vacancy, Co prefers a +2 high-spin valence state, whereas, at the bare surface and underneath water, it prefers a +3 intermediate and low-spin valence state, respectively.

The relatively low formation energies of the oxygen defects combined with the adsorption results indicate that the CFO (001)/(100) surfaces are hydroxylated under ambient conditions and that oxygen vacancies in CFO may be important active centers during catalytic redox reactions.

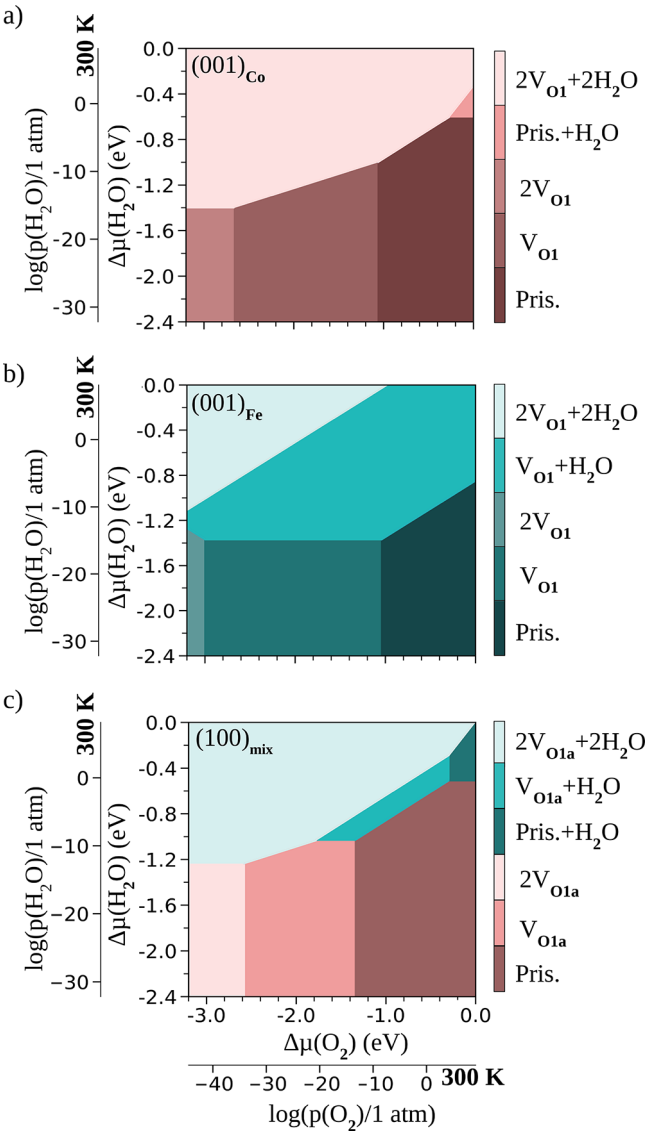


Figure 5. Surface phase diagrams for CFO (a) $(001)_{Co}$, (b) $(001)_{Fe}$, and (c) $(100)_{mix}$ surfaces exposed to water and O_2. Ambient conditions correspond to T = 300 K, $p(O_2)$ = 0.2 atm, and $p(H_2O)$ = 0.02 atm. $\Delta\mu(X)$ is the difference between the chemical potential of X (X = O_2, H_2O) and its total energy (i.e., $\Delta\mu(X) = \mu(X) - E_X$).

ASSOCIATED CONTENT

Supporting Information

The Supporting Information is available free of charge at https://pubs.acs.org/doi/10.1021/acs.jpcc.1c01881.

Cartesian coordinates of the slab unit cells of CFO and average displacements of the surface layers with respect to the positions in the bulk; computed spin *d*-orbital occupation numbers and density of states; structures of the surfaces with two oxygen vacancies; optimized structures of water adsorption on the (001)/(100) surfaces (PDF)

https://doi.org/10.1021/acs.jpcc.1c01881
J. Phys. Chem. C XXXX, XXX, XXX−XXX

AUTHOR INFORMATION

Corresponding Author

Arjeta Rushiti − *Department of Theoretical Chemistry, Ruhr University Bochum, D-44870 Bochum, Germany;* orcid.org/0000-0002-1178-6091; Email: Arjeta.Rushiti@ruhr-uni-bochum.de

Authors

Christof Hättig − *Department of Theoretical Chemistry, Ruhr University Bochum, D-44870 Bochum, Germany;* orcid.org/0000-0002-5752-2710

Bo Wen − *Department of Chemistry, Princeton University, Princeton, New Jersey 08544, United States; School of Physics and Electronics, Henan University, Kaifeng 475004, China;* orcid.org/0000-0001-7252-918X

Annabella Selloni − *Department of Chemistry, Princeton University, Princeton, New Jersey 08544, United States;* orcid.org/0000-0001-5896-3158

Complete contact information is available at: https://pubs.acs.org/10.1021/acs.jpcc.1c01881

Notes

The authors declare no competing financial interest.

ACKNOWLEDGMENTS

This work was funded by the Deutsche Forschungsgemeinschaft (DFG, German Research Foundation, project number 388390466−TRR 247). A.R. acknowledges financial support by the Ruhr University Research School PLUS, funded by Germany's Excellence Initiative [DFG GSC 98/3]. B.W. and A.S. were supported by DoE-BES, Division of Chemical Sciences, Geosciences and Biosciences under Award DESC-0007347. We used resources of the TIGRESS High Performance Computer Center at Princeton University.

REFERENCES

(1) Zhao, Q.; Yan, Z.; Chen, C.; Chen, J. Spinels: controlled preparation, oxygen reduction/evolution reaction application, and beyond. *Chem. Rev.* **2017**, *117*, 10121−10211.

(2) Kaczmarczyk, J.; Zasada, F.; Janas, J.; Indyka, P.; Piskorz, W.; Kotarba, A.; Sojka, Z. Thermodynamic stability, redox properties, and reactivity of Mn_3O_4, Fe_3O_4, and Co_3O_4 model catalysts for N_2O decomposition: resolving the origins of steady turnover. *ACS Catal.* **2016**, *6*, 1235−1246.

(3) Russo, N.; Fino, D.; Saracco, G.; Specchia, V. N_2O catalytic decomposition over various spinel-type oxides. *Catal. Today* **2007**, *119*, 228−232.

(4) Borah, B. J.; Yamada, Y.; Bharali, P. Unravelling the role of metallic Cu in Cu-$CuFe_2O_4$/C nanohybrid for enhanced oxygen reduction electrocatalysis. *ACS Appl. Energy Mater.* **2020**, *3*, 3488−3496.

(5) Mahala, C.; Sharma, M. D.; Basu, M. 2D Nanostructures of $CoFe_2O_4$ and $NiFe_2O_4$: efficient oxygen evolution catalyst. *Electrochim. Acta* **2018**, *273*, 462−473.

(6) Zhang, S.; Shan, J.; Nie, L.; Nguyen, L.; Wu, Z.; Tao, F. F. In situ studies of surface of $NiFe_2O_4$ catalyst during complete oxidation of methane. *Surf. Sci.* **2016**, *648*, 156−162.

(7) Reddy, G. K.; Gunasekera, K.; Boolchand, P.; Dong, J.; Smirniotis, P. G. High temperature water gas shift reaction over nanocrystalline copper codoped-modified ferrites. *J. Phys. Chem. C* **2011**, *115*, 7586−7595.

(8) Estrella, M.; Barrio, L.; Zhou, G.; Wang, X.; Wang, Q.; Wen, W.; Hanson, J. C.; Frenkel, A. I.; Rodriguez, J. A. In situ characterization of $CuFe_2O_4$ and Cu/Fe_3O_4 water- gas shift catalysts. *J. Phys. Chem. C* **2009**, *113*, 14411−14417.

(9) Moyer, J.; Vaz, C.; Negusse, E.; Arena, D.; Henrich, V. Controlling the electronic structure of $Co_{1-x}Fe_{2+x}O_4$ thin films through iron doping. *Phys. Rev. B: Condens. Matter Mater. Phys.* **2011**, *83*, 035121−10.

(10) Brabers, V. A. M. In *Handbook of Magnetic Materials*, 1st ed.; Buschow, K. H. J., Ed.; Chapter 3, Vol. *8*; Elsevier B. V.: Amsterdam, The Netherlands, 1995; pp 189−324.

(11) Chakrapani, K.; Bendt, G.; Hajiyani, H.; Schwarzrock, I.; Lunkenbein, T.; Salamon, S.; Landers, J.; Wende, H.; Schlögl, R.; Pentcheva, R.; et al. Role of composition and size of cobalt ferrite nanocrystals in the oxygen evolution reaction. *ChemCatChem* **2017**, *9*, 2988−2995.

(12) Chakrapani, K.; Bendt, G.; Hajiyani, H.; Lunkenbein, T.; Greiner, M. T.; Masliuk, L.; Salamon, S.; Landers, J.; Schlögl, R.; Wende, H.; et al. The role of composition of uniform and highly dispersed cobalt vanadium iron spinel nanocrystals for oxygen electrocatalysis. *ACS Catal.* **2018**, *8*, 1259−1267.

(13) Hajiyani, H.; Pentcheva, R. Surface termination and composition control of activity of the $Co_xNi_{1-x}Fe_2O_4$(001) surface for water oxidation: insights from DFT+ U calculations. *ACS Catal.* **2018**, *8*, 11773−11782.

(14) El Arrassi, A.; Liu, Z.; Evers, M. V.; Blanc, N.; Bendt, G.; Saddeler, S.; Tetzlaff, D.; Pohl, D.; Damm, C.; Schulz, S.; et al. Intrinsic activity of oxygen evolution catalysts probed at single $CoFe_2O_4$ nanoparticles. *J. Am. Chem. Soc.* **2019**, *141*, 9197−9201.

(15) Budiyanto, E.; Yu, M.; Chen, M.; DeBeer, S.; Rüdiger, O.; Tüysüz, H. Tailoring morphology and electronic structure of cobalt iron oxide nanowires for electrochemical oxygen evolution reaction. *ACS Appl. Energy Mater.* **2020**, *3*, 8583−8594.

(16) Anke, S.; Falk, T.; Bendt, G.; Sinev, I.; Hävecker, M.; Antoni, H.; Zegkinoglou, I.; Jeon, H.; Knop-Gericke, A.; Schlögl, R.; et al. On the reversible deactivation of cobalt ferrite spinel nanoparticles applied in selective 2-propanol oxidation. *J. Catal.* **2020**, *382*, 57−68.

(17) Hähsler, M.; Landers, J.; Nowack, T.; Salamon, S.; Zimmermann, M.; Heißler, S.; Wende, H.; Behrens, S. Magnetic properties and Mössbauer spectroscopy of Fe_3O_4/$CoFe_2O_4$ nanorods. *Inorg. Chem.* **2020**, *59*, 3677−3685.

(18) Ross, J. R. H. *Heterogeneous Catalysis: Fundamentals and Applications*; Chapter 6; Elsevier B. V.: Amsterdam, The Netherlands, 2012; pp 123−142.

(19) Giannozzi, P.; Baroni, S.; Bonini, N.; Calandra, M.; Car, R.; Cavazzoni, C.; Ceresoli, D.; Chiarotti, G. L.; Cococcioni, M.; Dabo, I.; et al. QUANTUM ESPRESSO: a modular and open-source software project for quantum simulations of materials. *J. Phys.: Condens. Matter* **2009**, *21*, 395502−19.

(20) Perdew, J. P.; Burke, K.; Ernzerhof, M. Generalized gradient approximation made simple. *Phys. Rev. Lett.* **1996**, *77*, 3865−3868.

(21) Shi, X.; Bernasek, S. L.; Selloni, A. Mechanism and activity of CO oxidation on (001) and (110) surfaces of spinel Co_3O_4, $NiCo_2O_4$ and $NiFe_2O_4$: A DFT+ U study. *Surf. Sci.* **2018**, *677*, 278−283.

(22) Selcuk, S.; Selloni, A. DFT+ U study of the surface structure and stability of Co_3O_4 (110): Dependence on U. *J. Phys. Chem. C* **2015**, *119*, 9973−9979.

(23) Vanderbilt, D. Soft self-consistent pseudopotentials in a generalized eigenvalue formalism. *Phys. Rev. B: Condens. Matter Mater. Phys.* **1990**, *41*, 7892−7895.

(24) Shi, X.; Bernasek, S. L.; Selloni, A. Formation, electronic structure, and defects of Ni substituted spinel cobalt oxide: a DFT+ U study. *J. Phys. Chem. C* **2016**, *120*, 14892−14898.

(25) Chase, M. W., Jr. *NIST-JANAF Thermochemical Tables*, 4th ed.; American Chemical Society and American Institute of Physics for the National Institute of Standards and Technology: Washington, D. C. and New York, 1998.

(26) Reuter, K.; Scheffler, M. Composition, structure, and stability of RuO_2 (110) as a function of oxygen pressure. *Phys. Rev. B: Condens. Matter Mater. Phys.* **2001**, *65*, 035406−11.

(27) Li, Z.; Fisher, E.; Liu, J.; Nevitt, M. Single-crystal elastic constants of Co-Al and Co-Fe spinels. *J. Mater. Sci.* **1991**, *26*, 2621−2624.

(28) Sharma, D.; Khare, N. Tuning of optical bandgap and magnetization of $CoFe_2O_4$ thin films. *Appl. Phys. Lett.* **2014**, *105*, 032404−4.
(29) Dileep, K.; Loukya, B.; Pachauri, N.; Gupta, A.; Datta, R. Probing optical band gaps at the nanoscale in $NiFe_2O_4$ and $CoFe_2O_4$ epitaxial films by high resolution electron energy loss spectroscopy. *J. Appl. Phys.* **2014**, *116*, 103505−8.
(30) Hou, Y.; Zhao, Y.; Liu, Z.; Yu, H.; Zhong, X.; Qiu, W.; Zeng, D.; Wen, L. Structural, electronic and magnetic properties of partially inverse spinel $CoFe_2O_4$: a first-principles study. *J. Phys. D: Appl. Phys.* **2010**, *43*, 445003−7.
(31) Sit, P. H.-L.; Car, R.; Cohen, M. H.; Selloni, A. Simple, unambiguous theoretical approach to oxidation state determination via first-principles calculations. *Inorg. Chem.* **2011**, *50*, 10259−10267.
(32) Blanca-Romero, A.; Pentcheva, R. Confinement-induced metal-to-insulator transition in strained $LaNiO_3/LaAlO_3$ superlattices. *Phys. Rev. B: Condens. Matter Mater. Phys.* **2011**, *84*, 195450−7.
(33) Quan, Y.; Pardo, V.; Pickett, W. E. Formal valence, 3d-electron occupation, and charge-order transitions. *Phys. Rev. Lett.* **2012**, *109*, 216401−5.
(34) Shi, X.; Bernasek, S. L.; Selloni, A. Oxygen deficiency and reactivity of spinel $NiCo_2O_4$ (001) surfaces. *J. Phys. Chem. C* **2017**, *121*, 3929−3937.
(35) Shi, X.; Li, Y.-F.; Bernasek, S. L.; Selloni, A. Structure of the $NiFe_2O_4$ (001) surface in contact with gaseous O_2 and water vapor. *Surf. Sci.* **2015**, *640*, 73−79.
(36) Honrao, S. J.; Rizzardi, Q.; Maaß, R.; Trinkle, D. R.; Hennig, R. G. Split-vacancy defect complexes of oxygen in hcp and fcc cobalt. *Phys. Rev. Mater.* **2020**, *4*, 103608−9.
(37) Anke, S.; Bendt, G.; Sinev, I.; Hajiyani, H.; Antoni, H.; Zegkinoglou, I.; Jeon, H.; Pentcheva, R.; Roldan Cuenya, B.; Schulz, S.; et al. Selective 2-propanol oxidation over unsupported Co_3O_4 spinel nanoparticles: mechanistic insights into aerobic oxidation of alcohols. *ACS Catal.* **2019**, *9*, 5974−5985.

https://doi.org/10.1021/acs.jpcc.1c01881
J. Phys. Chem. C XXXX, XXX, XXX−XXX